

# Single Layer $\text{PbI}_2$ : Hydrogenation-driven Reconstructions

C. Bacaksiz<sup>1</sup> and H. Sahin<sup>2</sup>

<sup>1</sup>*Department of Physics, Izmir Institute of Technology, 35430 Izmir, Turkey*

<sup>2</sup>*Department of Photonics, Izmir Institute of Technology, 35430 Izmir, Turkey*

(Dated: July 22, 2016)

## Abstract

By performing density functional theory-based calculations, we investigate how hydrogen atom interacts with the surfaces of monolayer  $\text{PbI}_2$  and how one and two side hydrogenation modify its structural, electronic, and magnetic properties. Firstly, it was shown that T-phase of single layer  $\text{PbI}_2$  is energetically favorable than the H-phase. It is found that hydrogenation of its surfaces is possible through the adsorption of each hydrogen on iodine sites. While H atoms do not form a particular bonding-type at low concentration, by increasing the number of hydrogenated I-sites well-ordered hydrogen patterns are formed on  $\text{PbI}_2$  matrix. In addition, we found that for one-side hydrogenation, the structure forms a  $(2 \times 1)$  Jahn-Teller type distorted structure and band gap is dramatically reduced compared to hydrogen-free single layer  $\text{PbI}_2$ . Moreover, in the case of full-hydrogenation, the structure also possesses another  $(2 \times 2)$  reconstruction with reduction in the band gap. Easy-tunable electronic and structural properties of single layer  $\text{PbI}_2$  by hydrogenation reveal its potential use in nanoscale semiconducting device applications.

PACS numbers: 73.20.Hb, 82.45.Mp, 73.61.-r, 73.90.+f, 74.78.Fk

## I. INTRODUCTION

After a decade of research which was triggered by the synthesis of graphene,<sup>1</sup> the theoretical prediction and synthesis of many 2D ultrathin materials such as silicene,<sup>4,5</sup> germanene,<sup>4,6,7</sup> stanene,<sup>8,9</sup> transition metal dichalcogenides (TMDs),<sup>10–17</sup> hexagonal III-V binary compounds (h-BN, h-AlN)<sup>18–21</sup> and metal hydroxides ( $\text{Ca}(\text{OH})_2$ ,  $\text{Mg}(\text{OH})_2$ )<sup>22,23</sup> have been achieved. However, recent research efforts have been directed towards not only synthesis of graphene-like materials, but also towards the functionalization of existing ultra-thin crystal structures. These recent studies have revealed some important results such as (i) tunable bandgap opening in graphene<sup>24–29</sup> (ii) H-defect-induced magnetization of graphane,<sup>29,30</sup> (iii) band gap engineering in silicene and germanene,<sup>31–33</sup> (iv) stability enhancement in h-BN,<sup>34</sup> (v) tunable magnetic features in TMDs.<sup>35,36</sup>

One of the most recently synthesized single layer semiconductor is lead iodide ( $\text{PbI}_2$ ). In bulk  $\text{PbI}_2$ , which is a member of metal halides family, van der Waals stacked individual layers are in the form of octahedral T-phase. As a precursor material for lead iodide perovskites, given by the general formula of  $\text{CH}_3\text{NH}_3\text{PbI}_{3-n}\text{X}_n$  ( $\text{X}=\text{Cl}, \text{Br}$ ),  $\text{PbI}_2$  has been used in many different device applications.<sup>37–41</sup> Recently, by performing the optical measurements and first-principles calculations of bulk and few-layer  $\text{PbI}_2$ , Toulouse *et al.* showed that exciton binding energy dramatically increases with a decreasing number of layers.<sup>42</sup> In addition, the synthesis of the monolayer  $\text{PbI}_2$  within the carbon nanotubes was reported by Cabana *et al.*<sup>43</sup> In a recent work, Zhou *et al.* investigated the structure, stability, electronic and optical properties of the monolayer  $\text{PbI}_2$  and also the hetero-bilayer form with graphene by using first principles calculations.<sup>44</sup> However, to our knowledge, the interaction between hydrogen (H) atom and the surface of monolayer  $\text{PbI}_2$  and how the physical properties are effected under hydrogenation are still open questions.

In this study, using first principles calculations based on density functional theory (DFT), we investigate the interaction of hydrogen atoms with bare single layer  $\text{PbI}_2$ . We also focus on structural and electronic properties of half- and fully-hydrogenated monolayers of  $\text{PbI}_2$ . We found that the T-phase is energetically more favourable than H-phase and it is an indirect semiconductor. Our investigation revealed that the chemical functionalization by both half- and full-hydrogenation cause reconstruction in the structure of monolayer  $\text{PbI}_2$  and lead to significant reduction in the band gap of the structure. Such a hydrogen-driven

reconstruction in monolayers of  $\text{PbI}_2$  have not been reported before.

The paper is organized as follows: in Sec. II we give details of our computational methodology. An overview of the structural phases and the electronic properties of monolayer hexagonal  $\text{PbI}_2$  are presented in Sec. III. In Sec. IV we focus on the interaction between the single hydrogen atom and the monolayer  $\text{PbI}_2$ . The effects of the one side hydrogen coverage, in other word half-hydrogenation, of monolayer  $\text{PbI}_2$  are given in Sec.V, and after that properties of fully-hydrogenated monolayer  $\text{PbI}_2$  are presented in Sec. VI. Finally, we present our conclusion in Sec. VII.

## II. COMPUTATIONAL METHODOLOGY

We perform the structural optimization and molecular dynamics (MD) simulations by using the Vienna ab-initio simulation package, VASP<sup>45-47</sup> which is based on density functional theory (DFT). To describe electron exchange and correlation The Perdew-Burke-Ernzerhof (PBE) form of the generalized gradient approximation (GGA)<sup>48</sup> was adopted. The vdW forces, which are effective on intralayer interaction, were taken into account by using the DFT-D2 method of Grimme.<sup>49,50</sup> To obtain the charge distribution of the configuration, a Bader charge analysis was used.<sup>51,52</sup> The stability of the resulting structures was examined with ab-initio MD calculations.

The following parameters were used for analyses. The total energy difference between the sequential steps in the iterations was taken  $10^{-5}$  units as convergence criterion. The convergence for the Hellmann-Feynman forces on each unitcell was taken to be  $10^{-4}$  eV/Å. 0.05 eV of Gaussian smearing factor was used and the pressures on the unit cell were decreased to a value less then 1.0 kB in all three directions. For the determination of accurate charge densities, Brillouin zone integration was performed using a  $12 \times 12 \times 1$   $\Gamma$ -centered mesh for the primitive unit cell. To avoid interactions between adjacent  $\text{PbI}_2$  configurations, our calculations were performed with a large unit cell including 16 Å vacuum space.

## III. H AND T PHASES OF SINGLE LAYER $\text{PbI}_2$

Similar to TMDs, monolayer  $\text{PbI}_2$  can form two different phases, octahedrally coordinated 1T and trigonal-prismatic coordinated 1H. As shown in Fig. 1, both phases have three

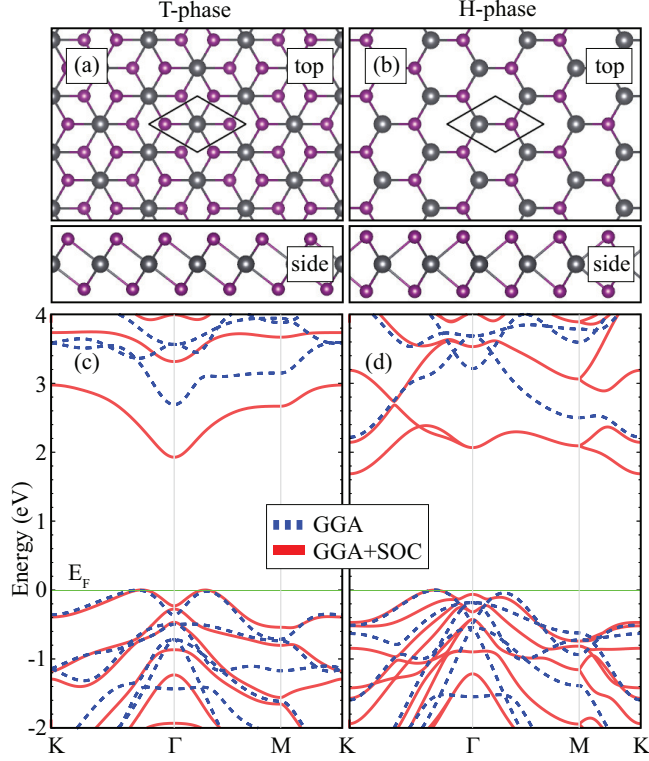


FIG. 1: (Color online) (a) and (b) illustrate the structure of monolayer 1T and 1H  $\text{PbI}_2$ , respectively. (c) and (d) are the corresponding band structures where the blue and red curves represent the GGA and GGA+SOC, respectively. The Fermi level ( $E_F$ ) is given by green solid line.

TABLE I: Calculated parameters for monolayer  $\text{PbI}_2$  are the lattice constant in the lateral direction,  $a$ ; the atomic distance Pb and I atoms,  $d_{\text{Pb-I}}$ ; the charge transfer from Pb to I atom,  $\Delta\rho$ ; the work function  $\Phi$ ; and the cohesive energy,  $E_c$ .  $E_g^{\text{GGA}}$  and  $E_g^{\text{GGA+SOC}}$  are the energy band gap values within GGA and GGA+SOC, respectively.

	$a$	$d_{\text{Pb-I}}$	$\Delta\rho$	$\Phi$	$E_c$	$E_g^{\text{GGA}}$	$E_g^{\text{GGA+SOC}}$
	(Å)	(Å)	( $e^-$ )	(eV)	(eV)	(eV)	(eV)
1T $\text{PbI}_2$	4.44	3.23	0.9	5.96	2.76	2.69	1.93
1H $\text{PbI}_2$	4.32	3.26	0.8	6.05	2.70	2.22	1.68

trigonal subplanes where the Pb subplane is sandwiched by two I-subplanes. While the 1T phase is a member of the  $P\bar{3}m2$  space group where subplanes of it are  $ABC$  stacked, the 1H is a member of the  $P\bar{6}m2$  space group where subplanes of it are  $ABA$  stacked. The lattice vectors of both phases are  $\mathbf{v}_1 = a(\frac{1}{2}, \frac{\sqrt{3}}{2}, 0)$ ,  $\mathbf{v}_2 = a(\frac{1}{2}, -\frac{\sqrt{3}}{2}, 0)$  where  $|\mathbf{v}_1| = |\mathbf{v}_2|$  and  $a$  is

the lattice constant. The atomic coordinates of 1T phase are  $(\frac{|v_1|}{2}, \frac{|v_1|}{2}, 0)$ ,  $(\frac{|v_1|}{6}, \frac{|v_1|}{6}, \frac{c}{2})$ , and  $(\frac{5|v_1|}{6}, \frac{5|v_1|}{6}, -\frac{c}{2})$  for the Pb and two I atoms, respectively, where  $c$  is the distance between the subplanes of I atoms. The atomic coordinates of 1H phase are given as  $(\frac{|v_1|}{3}, \frac{|v_1|}{3}, 0)$ ,  $(\frac{2|v_1|}{3}, \frac{2|v_1|}{3}, \frac{c}{2})$ , and  $(\frac{2|v_1|}{3}, \frac{2|v_1|}{3}, -\frac{c}{2})$ .

Lattice constants of the optimized crystal structures of 1T and 1H phases are 4.44 Å and 4.32 Å, respectively. However, as shown in Table I, interatomic distance  $d_{Pb-I}$  of T-phase (3.23 Å) is found to be shorter than H-phase (3.26 Å). Total energy calculations also reveal that the 1T phase is 165 meV per unit cell more favourable over the H-phase. The cohesive energies per atom of 1T and 1H phases are 2.76 and 2.70 eV, respectively. These results are consistent with the previous results which showed that the T-phase is the most favourable form of both bulk and monolayer crystals of  $PbI_2$ . In addition, the workfunctions ( $\Phi$ ) of 1T and 1H phases are calculated to be 5.96 eV and 6.05 eV, respectively.

We also present electronic energy band dispersions of 1T and 1H phases (approximated by GGA and GGA+SOC) in Figs. 1 (c) and (d), respectively. The 1T phase of  $PbI_2$  monolayer has an indirect band gap where the valence band maximum (VBM) is between the  $K$  and the  $\Gamma$  symmetry points and the conduction band minimum (CBM) is at the  $\Gamma$  point. As given in Table I, the energy bandgaps of 1T phase are 2.69 and 1.93 eV within GGA and GGA+SOC. Total charge donated by each Pb atom are 0.9 and 0.8  $e^-$  for 1T and 1H phases, respectively. Moreover, the 1H phase has also an indirect band gap where the VBM is between the  $K$  and the  $\Gamma$  points and CBM is at the  $K$  point. The band gap of 1H phase is calculated to be 2.22 eV within GGA and 1.68 eV within GGA+SOC.

It is seen that although the T and H phases have similar electronic characteristics at the valence band edges which are immeasurable by experimental tools such as ARPES, lattice parameter and the work function is unique feature of each phases. Discussions in the following chapters will be performed on the 1T-phase that corresponds to the ground state crystalline structure of single layer  $PbI_2$ .

#### IV. INTERACTION WITH SINGLE HYDROGEN

For engineering the structural, electronic and magnetic properties of a material, surface hydrogenation is an easy and powerful method. From theoretical point of view determination of the interaction between the  $PbI_2$  surface and H atoms is of importance.

For the calculation of adsorption and diffusion characteristics of H atom on the surface of monolayer  $\text{PbI}_2$  a  $3 \times 3$  supercell, which is enough to avoid the interaction between adjacent H atoms, is used. First of all, to determine the most favourable adsorption site of H atom, various initial positions over the surface are calculated; top-Pb site, midpoint of Pb-I bond, the top-I site and the sites in between these points. As shown in Fig. 2 (a), adsorption of hydrogen atom in the vicinity of I atom with the bond length of  $1.66 \text{ \AA}$  is much more preferable than adsorption on other lattice points. It is also seen that the formation of tilted I-H bond with the surface leads to slightly out-of-plane relaxation of the underlying I atom. Considering its spin polarized ground state in vacuum, the binding energy of single H atom is calculated to be  $0.32 \text{ eV}$  which is quite small compared to binding energy of H to graphene ( $0.98 \text{ eV}$ ).<sup>53</sup>

In addition, our Bader charge analysis reveal that bonded H atom preserves its  $1.0 e^-$ , on the other hand, the H bonded I atom has  $7.0 e^-$  in contrast with the other I atoms which have  $7.4 e^-$ . The displaced  $0.4 e^-$  from that particular I atom are shared by the nearest three Pb atoms. Our analysis reveals that the H atom do not form a bond when the vdW term excluded. Therefore, one can conclude the bonding type of H with  $\text{PbI}_2$  surface as a weak vdW type bonding.

The single H bonded system have midgap states which originate from H atom. When we consider these states, the band gap is  $0.21 \text{ eV}$  as shown in Fig 2 (c). There is one localized band near the Fermi level which have charge distribution as shown inset of Fig 2 (c). The system has a magnetic ground state with magnetic moment of  $1.0 \mu_B$ . It also appears that only the states around Fermi level have splitting due to hydrogen-induced magnetism.

To have more general picture of interaction between H atom and the monolayer  $\text{PbI}_2$ , we perform the diffusion barrier calculation which is shown in Fig. 2 (d). From the top of an I atom to top of its second nearest I atom, the energy difference plot shows that top of I atom possesses the minimum energy. The barrier to escape from the influence of I atom is around  $285 \text{ meV}$ . There are one local minimum on the path which coincide the center of triangle of I atoms over the Pb atom. In addition, considering the energy plot around the I atom as an harmonic potential, the jump frequency of H atom is estimated to be  $\nu \approx 0.191 \text{ GHz}$ . These results are consistent with the MD simulations reveal that at low temperatures (up to  $50 \text{ K}$ ), each single H rotates almost freely around the I atom. Although each H is bonded to underlying I, there is no certain preferable bonding direction with the  $\text{PbI}_2$  surface.

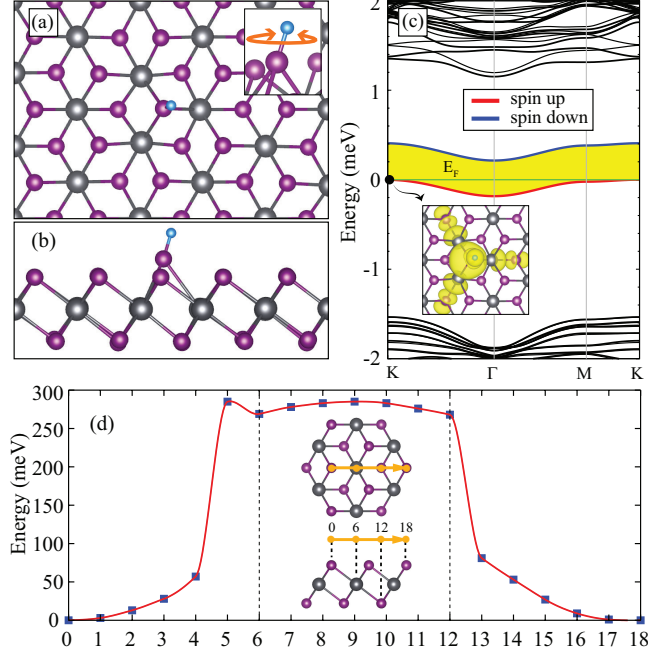


FIG. 2: (Color online) (a) and (b) show the structure of H atom adsorbed ( $3 \times 3$ )  $\text{PbI}_2$  from top and the side, respectively. The inset in (a) illustrates the rotation of H around the I atom. (c) is the band structure of single H atom adsorbed  $3 \times 3$   $\text{PbI}_2$  monolayer where the blue and red curves represent the spin-different states. Inset shows the charge distribution of VBM at the  $\Gamma$ . (d) is the diffusion barrier plot through the given path. The Fermi level ( $E_F$ ) is given by green solid line.

## V. ONE-SIDE HYDROGENATION

Following the analysis of the interaction of H atoms with the surfaces of  $\text{PbI}_2$ , in this section, we investigate how the structural, electronic and magnetic properties are modified upon the hydrogen coverage of surfaces. Firstly, the half-hydrogenated (half-H- $\text{PbI}_2$ ), one-by-one hydrogen coverage of each I atom on the same surface, structure is investigated.

As shown in Figs. 3 (a) and (b), H atoms form a well-ordered crystal structure (where  $\theta=60^\circ$ ) in the one-side covered structure. The lattice constant of this perfectly hexagonal crystal structure is calculated to be 4.05 Å. Compared to hydrogen-free bare  $\text{PbI}_2$  structure, Pb-I bond length increases from 3.23 to 3.77 Å at the hydrogenated side. However, at the hydrogen-free side, Pb-I bonds become stronger and the bond length is calculated to be 3.08 Å. Moreover, alongside with the structural changes, the half-hydrogenation also modifies charge distribution in the crystal structure. Bader charge analysis shows that

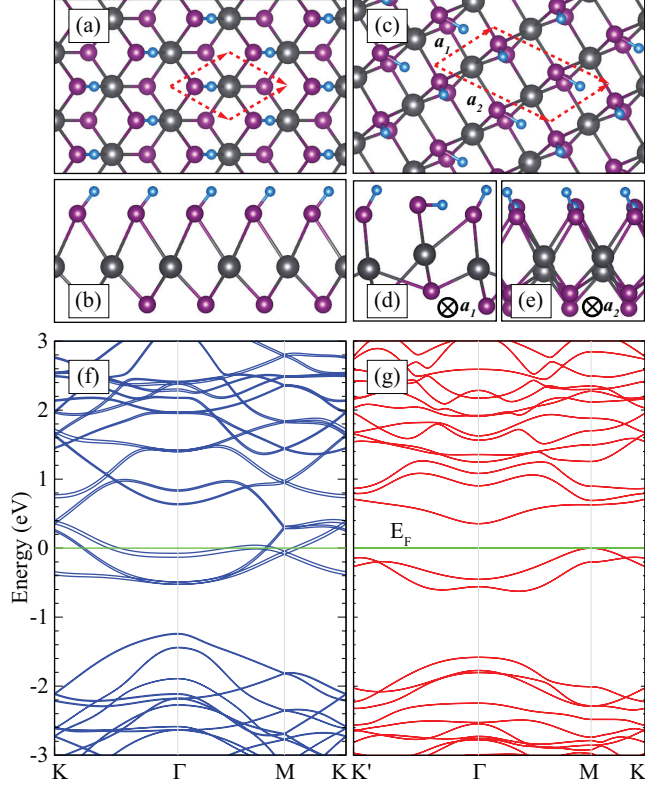


FIG. 3: (Color online) The structures in (a) and (b) for perfect hexagonal and (c), (d), and (e) for distorted forms of half-hydrogenated monolayer  $\text{PbI}_2$  (half-H- $\text{PbI}_2$ ), respectively. View direction are given in (d) and (e). (f) and (g) are the corresponding band structures. To compare the perfect and distorted forms,  $2 \times 2$  unitcells are used for both band structures. The Fermi level ( $E_F$ ) is given by green solid line.

functionalization cancels charge transfer between Pb and I atoms at the hydrogenated side and therefore, removes the ionic character of Pb-I bond. In contrast, at the bare side of the half-H- $\text{PbI}_2$ , the charge sharing increases where the I and Pb atoms have  $7.4$  and  $3.5 e^-$ , respectively. Electronically, as shown in Fig. 3 (f), the semiconducting character vanishes after hydrogenation and the system turns into a ferromagnetic metal with  $0.14 \mu_B$  per unitcell. However, hydrogenation-induced metalization in single layer  $\text{PbI}_2$  requires further analysis.

For further analysis of the half-hydrogenated structure we also perform finite temperature MD calculations. Our calculations showed that starting from very low temperatures (20-25 K) half-H- $\text{PbI}_2$  tends to undergo a structural transformation. Apparently, the perfectly hexagonal half-hydrogenated structure mentioned before corresponds to a local minimum on



TABLE II: Calculated parameters for half- and full-hydrogenated monolayer  $\text{PbI}_2$  (half-H- $\text{PbI}_2$  and full-H- $\text{PbI}_2$ ) are; the lattice constant in the lateral directions,  $\mathbf{a}_1$  and  $\mathbf{a}_2$ ; the angle between the lattice vectors,  $\theta$ ; the work function  $\Phi$ ; the cohesive energy,  $E_c$ ; the binding energy per H atom,  $E_{bind}$ ; the band gap,  $E_g^{\text{GGA}}$ ; and magnetic moment per primitive cell,  $\mu$ .

	$\mathbf{a}_1$	$\mathbf{a}_2$	$\theta$	$\Phi$	$E_c$	$E_{bind}$	$E_g^{\text{GGA}}$	$\mu$
	( $\text{\AA}$ )	( $\text{\AA}$ )	( $^\circ$ )	(eV)	(eV)	(eV)	(eV)	( $\mu_B$ )
half-H- $\text{PbI}_2$	4.22	7.83	58.9	3.57	2.23	0.64	0.35	0.0
full-H- $\text{PbI}_2$	8.29	8.02	63.0	3.73	2.03	0.93	0.76	0.0

Born-Oppenheimer surface and for the determination of the ground state structure one needs small perturbation such as temperature. Then, by performing full structural optimization of the distorted structure created by MD calculation, we obtained the real ground state crystal structure of half-H- $\text{PbI}_2$ .

As shown in Figs. 3 (c) and (d), the ground state of half-H- $\text{PbI}_2$  forms a  $(2 \times 1)$  reconstructed surface. It is calculated that this  $(2 \times 1)$  reconstructed phase of half-H- $\text{PbI}_2$  is 0.41 eV per unitcell more favourable than the perfectly hexagonal phase which is obtained by a total energy calculation performed at 0 K. In this half-H- $\text{PbI}_2$  structure, there are two bonding types of H atom. One H atom stands over the I atom with an angle of  $28.5^\circ$  with the normal of the structure plane, the other H reclines parallel to the surface at level of the I atoms. As given in Table II, the lattice constants are 4.22 and 7.83  $\text{\AA}$  with an angle of  $58.9^\circ$  and the workfunction at the hydrogenated side is found to be 3.57 eV. On the other side, the H binding energy per H atom is 0.64 eV which is much larger than that of single H on  $3 \times 3$  supercell ( $E_{bind}=0.32$  eV for single H).

The charge distributions of the reconstructed structure are specific for the structurally different Pb, I, and H atoms. In general, with respect to H atom bonding configurations, all atoms have specific charge in  $(2 \times 1)$  reconstructed unitcell (see Fig. 3 (c), (d), and (e)). Shortly, the standing- and reclining-H atoms have 1.1 and 1.0  $e^-$ ; the I atoms bonded with standing- and reclining-H have 7.0 and 7.1  $e^-$ ; the Pb atoms close to standing- and reclining-H have 3.4 and 3.7  $e^-$ , respectively. On the bare side of the half-H- $\text{PbI}_2$ , the I atoms have larger charge of 7.3 and 7.4  $e^-$  which are aligned in  $z$ -axis with standing- and reclining-H, respectively

Furthermore, upon the temperature-driven structural transformation from perfectly hexagonal to  $(2\times 1)$  reconstructed phase, not only the structure but also electronic properties are modified dramatically. As shown in Fig. 3 (g), the reconstruction removes the metallic property and the system becomes semiconductor with a small band gap of 0.35 eV. The band gap is still indirect in which the VBM and CBM are at M and  $\Gamma$  points, respectively. After the reconstruction the system has a nonmagnetic ground state. This type of distortions are known as Jahn-Teller distortion in which the dangling bonds are filled up and the system transforms from metal to semiconductor. Therefore, semiconducting nature of  $(2\times 1)$  reconstructed phase of half-H-PbI<sub>2</sub>, that corresponds to the ground state structure, is quite important for nanoscale optoelectronic device applications.

## VI. FULL HYDROGENATION

As well as one-side hydrogenation that may be realized on one-side-supported material, one can also achieve both-side coverage of monolayer PbI<sub>2</sub> (full-H-PbI<sub>2</sub>) when it is in free-standing form. Structural analysis of the full-H-PbI<sub>2</sub> is performed by applying the same methodology. MD calculations revealed that the ground state atomic structure of the full-H-PbI<sub>2</sub> is quite different from half-H-PbI<sub>2</sub>.

Similar to half-hydrogenated structure, H-induced reconstructions take place starting from 20-25 K and therefore three different types of I-H bonds (perpendicular, tilted bond with 44.8°, and the reclined parallel to the surface) are formed over the PbI<sub>2</sub> surface (see Figs. 4 (a), (b) and (c)). Then the analysis of fully-optimized crystal structure reveals that the primitive unitcell of full-H-PbI<sub>2</sub> contains a  $(2\times 2)$  reconstructed phase of PbI<sub>2</sub>H<sub>2</sub>. As given in the Table II, lattice parameters of the  $(2\times 2)$  reconstructed structure are calculated to be 8.29 and 8.02 Å with an angle of 63.0°.

Upon full hydrogenation, not only the structure but also work functions, cohesive energies and the H binding energies significantly differ from half-hydrogenated structure. The work function of the full-H-PbI<sub>2</sub> is found to be 3.73 eV. The cohesive energy of the full-H-PbI<sub>2</sub> is calculated to be 2.03 eV smaller than that of half-H-PbI<sub>2</sub>. The calculated average binding energy of an H atom is 0.93 eV which is larger as compared to those of single H and half-hydrogenated cases. Here, it is noteworthy that the larger binding energy is consistent with the slightly larger work function. As shown in Figs. 4 (d) the full-H-PbI<sub>2</sub> is a semiconductor

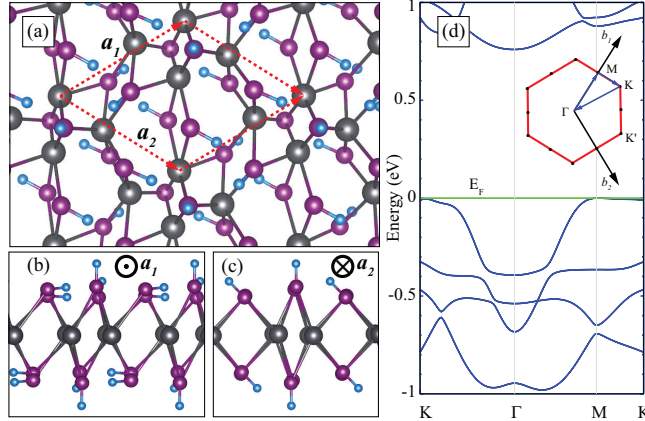


FIG. 4: (Color online) (a), (b), and (c) illustrate the structure of full-hydrogenated monolayer  $\text{PbI}_2$  from top, side views with the corresponding directions, respectively. (d) is the band structure of full-hydrogenated monolayer  $\text{PbI}_2$ . The Fermi level ( $E_F$ ) is given by green solid line.

with an indirect band gap of 0.76 eV. The VBM and CBM stay at M and  $\Gamma$  points which are similar to those of half-H- $\text{PbI}_2$ . It is also seen that the Jahn-Teller type distortion in the structure removes dangling bonds and therefore the system is converged to non-magnetic semiconducting ground state. ed

## VII. CONCLUSION

In this paper, we studied the newly emerging ultra-thin  $\text{PbI}_2$  which is a member of metal halides. Starting from the comparison of two possible monolayer phases, 1T and 1H, interaction with single H atom, half- and full-hydrogenation of monolayer  $\text{PbI}_2$  were investigated using first principles DFT calculations. The 1T phase was found to be favourable with the band gap of 2.69 and 1.93 eV within GGA and GGA+SOC, respectively. Our calculations also showed that the H atoms strongly reacts with the  $\text{PbI}_2$  surface and further functionalization of its surfaces can be realized. The binding energy was found to be 0.3 eV.

In the case of half-hydrogenation, it was found that the  $(2 \times 1)$  Jahn-Teller type distorted ground state structure corresponds to the ground state phase. We showed that reconstruction from perfectly hexagonal structure to  $2 \times 1$  half-H- $\text{PbI}_2$  leads to dramatical modifications such as (i) metal-to-semiconductor transition (ii) removal of magnetic moments . Moreover, our calculations revealed that full-hydrogenated monolayer  $\text{PbI}_2$  forms another  $(2 \times 2)$  Jahn-Teller distorted form in its ground state. In that case, the structure, full-H- $\text{PbI}_2$ , was a

nonmagnetic semiconductor with a bandgap of 0.76 eV. Our results reveal that hydrogenation is an efficient way to engineer the structural and electronic properties of single layer  $\text{PbI}_2$ .

### VIII. ACKNOWLEDGMENTS

This work was supported by the bilateral project between TUBITAK (through Grant No. 113T050) and the Flemish Science Foundation (FWO-VI). The calculations were performed at TUBITAK ULAKBIM, High Performance and Grid Computing Center (TR-Grid e-Infrastructure). CB and HS acknowledge the support from TUBITAK Project No 114F397. H.S. acknowledges support from Bilim Akademisi - The Science Academy, Turkey under the BAGEP program.

- 
- <sup>1</sup> K. S. Novoselov, A. K. Geim, S. V. Morozov, D. Jiang, Y. Zhang, S. V. Dubonos, I. V. Grigorieva, and A. A. Firsov, *Science* **306**, 666 (2004).
  - <sup>2</sup> M. Chhowalla, H. S. Shin, G. Eda, L-J Li, K. P. Loh, H Zhang, *Nat. Chem.* **5**, 263 (2013).
  - <sup>3</sup> C. Lee, X. Wei, J. W. Kysar, and J. Hone, *Science* **321**, 385 (2008).
  - <sup>4</sup> S. Cahangirov, M. Topsakal, E. Akturk, H. Sahin, and S. Ciraci, *Phys. Rev. Lett.* **102**, 236804 (2009).
  - <sup>5</sup> A. Kara, H. Enriquez, A. P. Seitsonen, L. C. L. Y. Voon, S. Vizzini, B. Aufray, and Hamid Oughaddou, *Surf. Science Report.* **67**, 1 (2012).
  - <sup>6</sup> M. E. Davila, L. Xian, S. Cahangirov, A. Rubio, and G. Le Lay, *New J. Phys.* **16** 095002 (2014).
  - <sup>7</sup> K. Yang, S. Cahangirov, A. Cantarero, A. Rubio, and R. D'Agosta, *Phys. Rev. B* **89**, 125403 (2014).
  - <sup>8</sup> G. G. Guzman-Verri and L. C. Lew Yan Voon, *Phys.Rev.B* **76**, 075131 (2007).
  - <sup>9</sup> F. Bechstedt, L. Matthes, P. Gori, and O. Pulci, *Appl. Phys. Lett.* **100**, 261906 (2012).
  - <sup>10</sup> R. A. Gordon, D. Yang, E. D. Crozier, D. T. Jiang, and R. F. Frindt, *Phys. Rev. B* **65**, 125407 (2002).
  - <sup>11</sup> J. N. Coleman, M. Lotya, A. O'Neill, S. D. Bergin, P. J. King, U. Khan, K. Young, A. Gaucher, S. De, R. J. Smith, I. V. Shvets, S. K. Arora, J. J. Boland, J. J. Wang, J. F. Donegan, J.

- C. Grunlan, G. Moriarty, A. Shmeliov, R. J. Nicholls, J. M. Perkins, E. M. Grieverson, K. Theuwissen, D. W. McComb, P. D. Nellist, and V. Nicolosi, *Science* **331**, 568 (2011).
- <sup>12</sup> C. Ataca, H. Sahin and S. Ciraci. *J. Phys. Chem. C*, **116** (16) 8983 (2012).
- <sup>13</sup> J. S. Ross, P. Klement, A. M. Jones, N. J. Ghimire, J. Yan, D. G. Mandrus, T. Taniguchi, K. Watanabe, K. Kitamura, W. Yao, D. H. Cobden, and X. Xu, *Nature Nanotech.* **9** 268 (2014).
- <sup>14</sup> H. Sahin, S. Tongay, S. Horzum, W. Fan, J. Zhou, J. Li, J. Wu, and F. M. Peeters, *Phys. Rev. B* **87**, 165409 (2013).
- <sup>15</sup> S. Tongay, H. Sahin, C. Ko, A. Luce, W. Fan, K. Liu, J. Zhou, Y.-S. Huang, C.-H. Ho, J. Yan, D. F. Ogletree, S. Aloni, J. Ji, S. Li, J. Li, F. M. Peeters, and J. Wu, *Nat. Comm.* **5** 3252 (2014).
- <sup>16</sup> S. Horzum, D. Cakir, J. Suh, S. Tongay, Y.-S. Huang, C.-H. Ho, J. Wu, H. Sahin, and F. M. Peeters, *Phys. Rev. B* **89**, 155433 (2014).
- <sup>17</sup> B. Chen, H. Sahin, A. Suslu, L. Ding, M. I. Bertoni, F. M. Peeters, and S. Tongay, *ACS Nano* **9**, 5326 (2015).
- <sup>18</sup> H. Sahin, S. Changirov, M. Topsakal, E. Bekaroglu, E. Akturk, R. T. Senger, and S. Ciraci, *Phys. Rev. B* **80**, 155453 (2009).
- <sup>19</sup> K. K Kim, A. Hsu, X. Jia, S. M. Kim, Y. Shi, M. Hofmann, D. Nezich, J. F. Rodriguez-Nieva, M. Dresselhaus, T. Palacios, and J. Kong, *Nano Lett.* **12**, 161 (2012).
- <sup>20</sup> P. Tsipas, S. Kassavetis, D. Tsoutsou, E. Xenogiannopoulou, E. Golias, S. A. Giamini, C. Grazianetti, D. Chiappe, A. Molle, M. Fanciulli, and A. Dimoulas, *Appl. Phys. Lett.* **103**, 251605 (2013).
- <sup>21</sup> C. Bacaksiz, H. Sahin, H. D. Ozaydin, S. Horzum, R. T. Senger, and F. M. Peeters, *Phys. Rev. B* **91**, 085430 (2015).
- Aierken, Suslu
- <sup>22</sup> Y. Aierken, H. Sahin, F. Iyikanat, S. Horzum, A. Suslu, B. Chen, R. T. Senger, S. Tongay, and F. M. Peeters, *Phys. Rev. B* **91**, 245413 Published 12 June 2015
- <sup>23</sup> A. Suslu, K. Wu, H. Sahin, B. Chen, S. Yang, H. Cai, T. Aoki, S. Horzum, J. Kang, F. M. Peeters, and S. Tongay, *Sci. Rep.* **6**, 20525 (2016).
- <sup>24</sup> D. C. Elias, R. R. Nair, T. M. G. Mohiuddin, S. V. Morozov, P. Blake, M. P. Halsall, A. C. Ferrari, D. W. Boukhvalov, M. I. Katsnelson, A. K. Geim, and K. S. Novoselov, *Science* **323**, 610 (2009).

- <sup>25</sup> M. Z. S. Flores, P. A. S. Autreto, S. B. Legoas, and D. S. Galvao, *Nanotechnology* **20**, 465704 (2009).
- <sup>26</sup> H. Sahin, C. Ataca, and S. Ciraci, *Phys. Rev. B* **81**, 205417 (2010).
- <sup>27</sup> H. Sahin, and C. Ciraci, *Phys. Rev. B* **84**, 035452 (2011).
- <sup>28</sup> J. O. Sofo, A. S. Chaudhari, and G. D. Barber, *Phys. Rev. B* **75**, 153401 (2007).
- <sup>29</sup> H. Sahin, C. Ataca, and S. Ciraci, *Appl. Phys. Lett.* **95**, 222510 (2009).
- <sup>30</sup> J Zhou, M. M. Wu, X. Zhou, and Q. Sun, *Appl. Phys. Lett.* **95**, 103108 (2009).
- <sup>31</sup> X.-Q. Wang, H.-D. Li, and J.-T. Wang, *Phys. Chem. Chem. Phys.* **14**, 3031 (2012).
- <sup>32</sup> L. C. Lew Yan Voon, E. Sandberg, R. S. Aga, and A. A. Farajian, *Appl. Phys. Lett.* **97**, 163114 (2010).
- <sup>33</sup> M. Houssa, E. Scalise, K. Sankaran, G. Pourtois, V. V. Afanasev, and A. Stesmans, *Appl. Phys. Lett.* **98**, 223107 (2011).
- <sup>34</sup> I. Cabria, M. J. Lopez, and J. A. Alonso, *Nanotechnology* **17**, 778 (2006).
- <sup>35</sup> H. Shi, H. Pan, Yo.-W. Zhang, and B. I. Yakobson *Phys. Rev. B* **88**, 205305 (2013).
- <sup>36</sup> H. Pan, *J. Phys. Chem. C* **118**, 13248 (2014).
- <sup>37</sup> M. M. Lee, J. Teuscher, T. Miyasaka, T. N. Murakami, and H. J. Snaith, *Science*, **338**, 643 (2012).
- <sup>38</sup> J. Y. Jeng, Y. F. Chiang, M. H. Lee, S. R. Peng, T. F. Guo, P. Chen, and T. C. Wen, *Adv. Mater.* **25**, 3727 (2013).
- <sup>39</sup> Z. K. Tan, R. S. Moghaddam, M. L. Lai, P. Docampo, R. Higler, F. Deschler, M. Price, A. Sadhanala, L. M. Pazos, D. Credginton, F. Hanusch, T. Bein, H. J. Snaith, and R. H. Friend, *Nat. Nanotechnol.* **9**, 687 (2014).
- <sup>40</sup> M. A. Green, A. Ho-Baillie and H. J. Snaith, *Nat. Photonics*, **8**, 506 (2014).
- <sup>41</sup> Y. Guo, K. Shoyama, W. Sato, Y. Matsuo, K. Inoue, K. Harano, C. Liu, H. Tanaka, and Eiichi Nakamura, *J. Am. Chem. Soc.* **137**, 15907 (2015).
- <sup>42</sup> A. S. Toulouse, B. P. Isaacoff, G. Shi, M. Matuchova, E. Kioupakis, and R. Merlin, *Phys. Rev. B* **91**, 165308 (2015).
- <sup>43</sup> L. Cabana, E. Batista, B. Ballesteros, C. Magn, R. Arenal, J. Or-Sol, R. Rurali, and G. Tobias, *Adv. Mater.* **26**, 2016 (2014).
- <sup>44</sup> M. Zhou, W. Duan, Y. Chen, and Aijun Du, *Nanoscale*, **7**, 15168 (2015).
- <sup>45</sup> G. Kresse and J. Hafner, *Phys. Rev. B* **47**, 558 (1993).

- <sup>46</sup> G. Kresse and J. Furthmüller, Phys. Rev. B **54**, 11169 (1996).
- <sup>47</sup> G. Kresse and D. Joubert, Phys.Rev.B **59**, 1758 (1999).
- <sup>48</sup> J. P. Perdew, K. Burke, and M. Ernzerhof, Phys. Rev. Lett. **77**, 3865 (1996).
- <sup>49</sup> S. J. Grimme, Comput. Chem. **27**, 1787 (2006).
- <sup>50</sup> T. Bucko, J. Hafner, S. Lebegue, and J. G. Angyan, J. Phys. Chem. A **114**, 11814 (2010).
- <sup>51</sup> G. Henkelman, A. Arnaldsson, and H. Jonsson, Comput. Mater. Sci. **36**, 354 (2006).
- <sup>52</sup> R. F. W. Bader, Atoms in Molecules A Quantum Theory (Oxford University Press, Oxford, UK, 1990).
- <sup>53</sup> H. Sahin and S. Ciraci, J. Phys. Chem. C **116**, 24075 (2012).